



McGillen, M., Curchod, B., Chhantyal Pun, R., Beames, J. M., Watson, N. P., Khan, A., ... Orr-Ewing, A. (2017). Criegee intermediate: alcohol reactions, a potential source of functionalized hydroperoxides in the atmosphere. *ACS Earth and Space Chemistry*. DOI: 10.1021/acsearthspacechem.7b00108

Peer reviewed version

Link to published version (if available):
[10.1021/acsearthspacechem.7b00108](https://doi.org/10.1021/acsearthspacechem.7b00108)

[Link to publication record in Explore Bristol Research](#)
PDF-document

This is the author accepted manuscript (AAM). The final published version (version of record) is available online via ACS at <http://pubs.acs.org/doi/abs/10.1021/acsearthspacechem.7b00108> . Please refer to any applicable terms of use of the publisher.

University of Bristol - Explore Bristol Research

General rights

This document is made available in accordance with publisher policies. Please cite only the published version using the reference above. Full terms of use are available:
<http://www.bristol.ac.uk/pure/about/ebr-terms.html>

1 **Title:**

2 Criegee Intermediate–Alcohol Reactions, A Potential Source of Functionalized Hydroperoxides in the
3 Atmosphere

4 **Author list:**

5 Max R. McGillen^{a,1}, Basile F.E. Curchod^a, Rabi Chhantyal-Pun^a, Joseph M. Beames^b, Nathan
6 Watson^b, M. Anwar H. Khan^a, Laura McMahon^a, Dudley E. Shallcross^a and Andrew J. Orr-Ewing^{a,1}

7 ^aSchool of Chemistry, University of Bristol, Cantock's Close, Bristol, BS8 1TS, UK; ^bSchool of
8 Chemistry, Cardiff University, Cardiff, CF10 3AT, UK

9 ¹To whom correspondence may be addressed. Email: max.mcgillen@gmail.com, a.orr-
10 ewing@bristol.ac.uk

11 **Keywords:**

12 Criegee, alcohol, kinetics, atmospheric chemistry, non-Arrhenius, hydroperoxide

13

14

15

16

17

18

19

20

21

22

23

24

25

26

27

28 **Abstract**

29 Ozonolysis, the mechanism by which alkenes are oxidized by ozone in the atmosphere, produces a
30 diverse family of oxidants known as Criegee intermediates (CIs). Using a combination of newly
31 acquired laboratory data and global atmospheric chemistry and transport modelling, we find that the
32 reaction of CIs with alcohols – a reaction that was originally employed to trap these reactive species
33 and provide evidence for the ozonolysis mechanism nearly 70 years ago – is occurring in Earth’s
34 atmosphere and may represent a sizeable source of functionalized hydroperoxides therein. Rate
35 coefficients are reported for the reactions of CH_2OO and $(\text{CH}_3)_2\text{COO}$ + methanol and that of CH_2OO
36 + ethanol. Substitution about the Criegee intermediate is found to have a strong influence over the
37 reaction rate, whereas substitution on the alcohol moiety does not. Although these reactions are not
38 especially rapid, both the precursors to CIs and alcohols have large emissions from the terrestrial
39 biosphere, leading to a high degree of collocation for this chemistry. We estimate that the products of
40 these reactions, the α -alkoxyalkyl hydroperoxides (AAAHs) have a production rate of $\sim 30 \text{ Gg yr}^{-1}$. In
41 order to assess the atmospheric lifetime of AAAHs, we used the nuclear ensemble method to
42 construct a UV absorption spectrum from the four lowest energy conformers identified for a
43 representative AAAH, methoxymethyl hydroperoxide. The computed absorption cross section
44 indicates that these compounds will be lost by solar photolysis, although not so rapidly as to exclude
45 competition from other sinks such as oxidation, thermal decay and aerosol uptake.

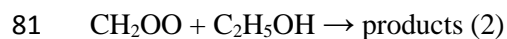
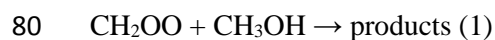
46 **1. Introduction**

47 Criegee intermediates (CIs), also known as carbonyl oxides, are a family of oxidants produced in
48 Earth’s atmosphere through alkene ozonolysis. The identity of a CI is determined by the alkene
49 reagent, and as a consequence of its zwitterionic character, may exist in several forms with significant
50 barriers to rotation between conformers.¹ In the ozonolysis of isoprene, for example, nine possible
51 Criegee intermediates are produced.² The corollary of this is that the variety of CIs encountered in the
52 atmosphere may exceed that of alkenes. Ozonolysis forms CIs that possess a range of internal
53 energies, a varying proportion of which possess sufficient excitation for prompt decomposition. The
54 remainder may be either collisionally stabilized or formed in a stabilized state. These stabilized CIs
55 will be sufficiently long-lived with respect to unimolecular processes that they may also engage in
56 bimolecular reactions.

57 Laboratory studies have identified a large diversity in the bimolecular reactivity among CIs. In the
58 case of water dimer, $(\text{H}_2\text{O})_2$, a rapid reaction ($k_{298} = 7.4 \times 10^{-12} \text{ cm}^3 \text{ molecule}^{-1} \text{ s}^{-1}$) is observed with
59 formaldehyde oxide, CH_2OO ,³ yet no significant reactivity ($k_{298} < 1.5 \times 10^{-16} \text{ cm}^3 \text{ molecule}^{-1} \text{ s}^{-1}$) is
60 observed for acetone oxide, $(\text{CH}_3)_2\text{COO}$.⁴ Conversely, both CIs react rapidly with SO_2 , with
61 $(\text{CH}_3)_2\text{COO}$ exhibiting a faster reaction rate.^{4,5} It is therefore apparent that the reactivity of a given CI
62 depends strongly upon both its structure and the identity of its reaction partner.

63 Despite having a low tropospheric concentration, estimated to be $5 \times 10^{4\pm 1}$ molecule cm^{-3} ,⁶ CIs have
64 been identified as important oxidants of both SO_2 ⁷⁻⁸ and organic acids.⁹⁻¹⁰ Furthermore, among
65 atmospheric oxidants, CIs are unusual in their capacity to add both carbon and oxygen mass to the co-
66 reactant through 1,3-dipolar cycloaddition¹¹⁻¹² and insertion mechanisms,¹³⁻¹⁴ and therefore have the
67 potential to produce low volatility products in comparatively few reaction steps, which may facilitate
68 secondary organic aerosol (SOA) formation.

69 Alcohols are a prevalent class of volatile organic compounds in the atmosphere and have terrestrial
70 biogenic sources,¹⁵⁻¹⁶ of which tropical rainforests are among the largest. Since the highest flux of CIs
71 is predicted to occur in the equatorial regions,^{9, 17} collocation is expected between CIs and alcohols in
72 the troposphere, and the reactions between these species therefore warrant investigation. Such
73 reactions are well known to synthetic chemists and have found utility in the preparation of α -
74 alkoxyalkyl hydroperoxides (AAAHs).¹⁸ Similarly in the gas phase, AAAHs have been identified in
75 the reaction of CIs (CH_2OO , *syn-/anti*-tridecanal oxide) with alcohols (methanol, 2-propanol), all of
76 which were studied using a static reaction chamber.¹⁹⁻²⁰ Tobias and Ziemann²⁰ reported a relative rate
77 coefficient for these reactions, where heptanoic acid was used as a reference compound. However,
78 few direct kinetic data are available and in order to address this knowledge gap, a systematic study of
79 the following reactions is conducted:



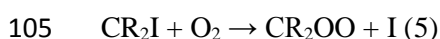
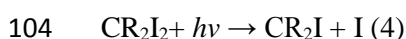
83 Reaction 1 is an insertion reaction and the product has been identified as methoxymethyl
84 hydroperoxide (MMHP).¹⁹ A calculated UV absorption spectrum of MMHP is presented, which
85 allows its atmospheric photolysis lifetime to be assessed. This spectrum is found to closely resemble
86 the experimentally measured spectra of analogous hydroperoxide species, and given the apparently
87 generic similarity between these hydroperoxides, MMHP is used to represent the panoply of AAAHs
88 that are expected to form from the reactions of larger, naturally occurring CIs with methanol. The
89 atmospheric implications of these reactions are investigated through global chemistry transport
90 modelling.

91 **2. Methods**

92 **2.1. Experimental measurements.** Rate coefficients for Reactions 1–3 were determined at
93 temperatures from 254–329 K and total pressures from 10–100 Torr using cavity ring-down
94 spectroscopy (CRDS) to obtain temporal decay profiles of a flowing mixture of CH_2OO or
95 $(\text{CH}_3)_2\text{COO}$ in the presence of a known excess of either methanol or ethanol. All rate coefficients

96 were measured under *pseudo*-first-order conditions, where [alcohol] \gg [CI]. The temperature of the
97 reactor was controlled by circulating a heated or cooled fluid through an outer jacket, with a second
98 insulating jacket employed to reduce temperature gradients across the reaction volume. A brief
99 description of the apparatus and experimental technique is given below, with a fuller account provided
100 by Chhantyal-Pun et al.^{5, 10}

101 Criegee intermediates, CH₂OO and (CH₃)₂COO were generated through the photolysis ($\lambda = 355$ nm)
102 of alkyl *gem*-diiodide precursors in the presence of excess O₂ according to the methodology of Welz
103 et al.²¹



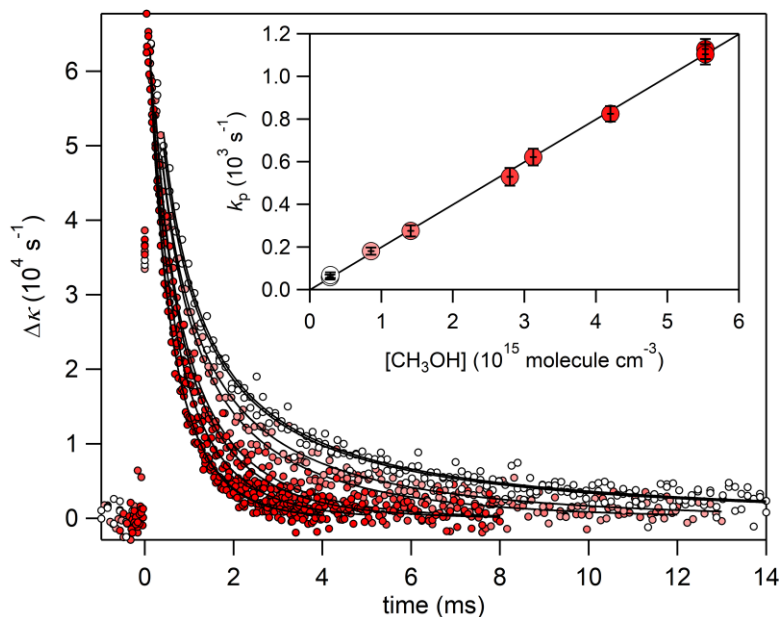
106 where R = H or CH₃.

107 Signals of CH₂OO or (CH₃)₂COO were probed using CRDS, the optical cavity of which was
108 positioned at an angle of 3.8° with respect to the photolysis beam, providing a 7.6 cm long interaction
109 region. The probe beam wavelength of 355 nm overlapped the broad and intense $\tilde{B}^1A' \leftarrow \tilde{X}^1A'$
110 electronic absorption bands of these CIs. Temporal decay profiles of CIs were generated by varying
111 the delay time (i.e. reaction time) between the photolysis and probe beams. Under our experimental
112 conditions, typical ring-down times (<6 μ s) were much shorter than the timescales over which kinetic
113 measurements were performed (1–14 ms).

114 These profiles were fitted with a simultaneous first- and second-order decay fit function shown in Eq.
115 I:⁵

116
$$\Delta\kappa(t) = \frac{k_p}{\frac{k_p}{\Delta\kappa(t_0)}e^{k_p t} - k' \left(\frac{2L}{cd}\right) + k' \left(\frac{2L}{cd}\right)e^{k_p t}} \quad (\text{I})$$

117 where $\Delta\kappa(t)$ is the change in ring-down decay rate constant at delay time t caused by the photolysis
118 laser, L is the cavity length (100 cm), d is the photolysis-probe laser overlap length (7.6 cm), c is the
119 speed of light, k_p is the *pseudo*-first-order rate coefficient with respect to the alcohol reagent, $k' = k_{\text{obs}}/$
120 $\sigma_{355 \text{ nm}}$ is the second-order decay rate coefficient for the self-reaction of the CI scaled by its absorption
121 cross section at 355 nm. Because k' is temperature dependent, a series of decay profiles were
122 measured in the absence of alcohol over a range of temperatures, and these data were used to define a
123 temperature-dependent function of the self-reaction, $k'(T)$, for use in this equation.



124

125 **Fig. 1.** A series of kinetic decay traces acquired at 254 K showing progressively faster decays of
 126 CH_2OO as methanol concentration is increased. Solid lines are fits according to Eq. I, from which the
 127 *pseudo*-first-order rate coefficients, k_p , are obtained. These values are plotted as a function of
 128 $[\text{CH}_3\text{OH}]$ in the inset, the slope of which yields the bimolecular rate coefficient. Error bars in the inset
 129 represent the 2σ statistical uncertainty of the fits.

130

131 Alcohols were introduced into the reaction volume from a dilute bulb using a calibrated flow
 132 controller (MKS) over a range of concentrations, typically spanning a factor of ≥ 20 . Concentrations
 133 were determined from the ideal gas law using the known mass flow rates from manometrically
 134 prepared bulbs, reactor temperature and pressure. Bimolecular rate coefficients for Reactions 1–3
 135 were obtained from the slope of an error-weighted linear least-squares fit of k_p vs [alcohol]. In
 136 experiments with CH_3OD and CD_3OD , since they possess the labile O–D moiety, D_2O was bubbled
 137 through the gas lines, mass flow controller and reactor for 24 hours prior to data acquisition.

138 **2.2. Materials.** Methanol ($\geq 99.9\%$), ethanol ($\geq 99.5\%$) CD_3OD (≥ 99.8 atom % D), CD_3OH (99.8 atom
 139 % D), CH_3OD (99.5 atom % D), diiodomethane (99%) (Sigma-Aldrich), 2,2-diiodopropane (a high-
 140 purity sample was synthesized at the University of Edinburgh, see SI for proton and carbon NMR
 141 spectra) were subjected to several freeze-pump-thaw cycles prior to their introduction into darkened
 142 10 L Pyrex bulbs. D_2O (99.9 atom % D) (Sigma-Aldrich) was degassed but otherwise used as
 143 supplied. High purity compressed gases N_2 (diluent and bath gas) and O_2 (reagent in Reaction 5) (Air
 144 Liquide) were used as supplied.

145 **2.3. Computational calculations.** For energy calculations, stationary points on the reaction pathways
 146 were optimized using DFT//B3LYP/aug-cc-pVTZ, all of which were verified through vibrational
 147 frequency calculations, and all transition states were linked to their respective minima through

148 intrinsic reaction coordinate calculations. All geometries were generated using the Gaussian09
149 package.²² Single point energy calculations were performed at each stationary point using DF-
150 HF//DF-LCCSD(T)-F12a/aug-cc-pVTZ. Both density fitting integral approximations, and local
151 correlation methods offer significant advantages in reducing computational cost when scaling to
152 larger molecular systems, and were used here to provide high accuracy molecular energies. These
153 calculations also include explicit electron correlation through use of the F12 ansatz, where F12a was
154 chosen as the most appropriate treatment for this basis set. All energy calculations were performed
155 using MOLPRO.²³ Recent calculations suggest that the CI moiety transitions from predominantly
156 zwitterionic to biradical character during the course of a bimolecular reaction,²⁴ which represents a
157 major challenge for most computational electronic structure techniques. Multireference computational
158 methods could be used in future for more detailed reaction pathway characterisation.

159 For calculation of absorption cross sections, geometry optimizations of MMHP were conducted at the
160 MP2 level of theory²⁵⁻²⁸ using an aug-cc-pVTZ basis set²⁹ with Gaussian09²² for four conformers (see
161 SI for details about the conformers and the level of theory employed). Frequency calculations
162 confirmed that all localized extrema are actual minima of the ground state potential energy surface. A
163 photoabsorption cross section was then constructed for each conformer using the semiclassical³⁰⁻³²
164 nuclear ensemble method as implemented in Newton-X version 1.4.³³⁻³⁴ The nuclear ensemble
165 technique samples a set of N_n nuclear geometries (200 in this case) from an approximate quantum
166 distribution in the ground-electronic state. Excitation energies (ΔE_{0n}) and oscillator strengths (f_{0n}) are
167 then computed for each sampled geometry \mathbf{R}_l and a photoabsorption cross section $\sigma(E)$ is constructed
168 by summing all the contributions using the equation:

$$169 \quad \sigma(E) = \frac{\pi e^2 \hbar \gamma}{2 m c \epsilon_0} \sum_n^{N_s} \frac{1}{N_n} \sum_l^{N_n} f_{0n}(\mathbf{R}_l) g(E - E_{0n}(\mathbf{R}_l), \delta) \quad (\text{II})$$

170 N_s is the total number of excited electronic states considered (1 in the present case) and
171 $g(E - E_{0n}(\mathbf{R}_l), \delta)$ corresponds to a Lorentzian function with a width $\delta = 0.05$ eV. The nuclear
172 ensemble technique provides band shapes and heights, but it is important to note that it does not
173 reproduce vibronic progressions.

174 The excitation energies and oscillator strengths for the transition to the first electronic state (S_1) were
175 computed for all sampled geometries with the spin-component scaling second-order approximate
176 coupled cluster (SCS-CC2) method,³⁵⁻³⁷ using an aug-cc-pVDZ basis set, with the program
177 Turbomole v6.4.³⁸ This level of theory was benchmarked against equation-of-motion coupled cluster
178 singles and doubles (EOM-CCSD),³⁹ and a detailed comparison is presented in the supporting
179 information.

180 **2.4. Atmospheric chemistry and transport modelling.** The atmospheric sources of AAAHs were
181 quantified by incorporating the kinetic measurements of this study into the STOCHEM-CRI global

182 atmospheric chemistry and transport model.⁴⁰ In the model, CIs are generated from 6 representative
183 alkenes (ethene, propene, (*Z*)-2-butene, isoprene, α -pinene and β -pinene). Since many more alkenes
184 are emitted to the atmosphere than are present in the model, this limited selection is weighted to
185 reflect the alkene functionality of the total biogenic alkene flux into the atmosphere,⁴¹ which allows
186 for a realistic distribution of CIs at a reduced computational cost. Both the model and the
187 methodology for generating CI fields have been used previously.^{9,42} However, based on the
188 availability of new experimental measurements and quantum calculations, these CI fields have been
189 updated.¹⁰ A full account of the stabilized CI yield from ozonolysis, the branching ratio between CIs,
190 the unimolecular loss rate and rate coefficients for reactions with H₂O, (H₂O)₂ and methanol for each
191 of the CIs contained within the model is provided in Table S4. By considering the production through
192 the reactions of CIs with alcohols and the losses by photolysis and reaction with OH (by analogy to
193 other hydroperoxides), the concentration of AAAH can be estimated in the model.

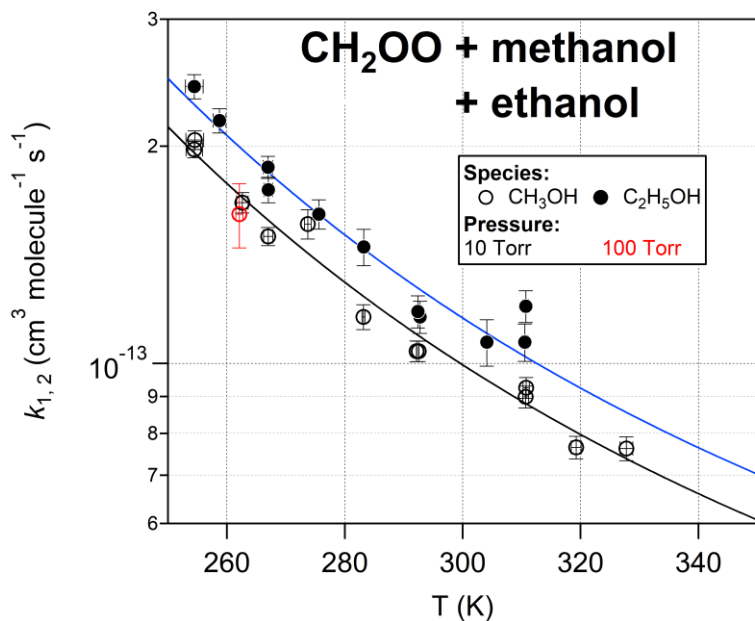
194 **3. Experimental results**

195 Experiments were conducted to measure the rates of reaction of CIs with methanol and ethanol. All
196 kinetic data were fitted using a combined 1st- and 2nd-order expression, Eq. I (see Section 2.1) and
197 temporal profiles of CIs were well described by these fits in all cases (Fig. 1 shows a representative
198 dataset). In the experiments in which (CH₃)₂COO was a reagent, a more rapid unimolecular decay
199 occurred ($\sim 300\text{ s}^{-1}$)⁴³, which manifested itself as an intercept in plots of k_p vs [methanol]. Rate
200 coefficients were observed to be pressure independent from 10–100 Torr (N₂). Rate coefficient data
201 are plotted as a function of temperature in Figs. 2–3, and show that Reactions 1–3 each exhibit a
202 negative temperature dependence, together with curvature, which is quite pronounced in the case of
203 Reaction 3. Kinetic data obtained in this study are presented in Tables S1–3, together with the
204 experimental conditions that were employed; errors in rate coefficients are expressed as 2σ statistical
205 uncertainty, other errors are provided at 1σ .

206

207

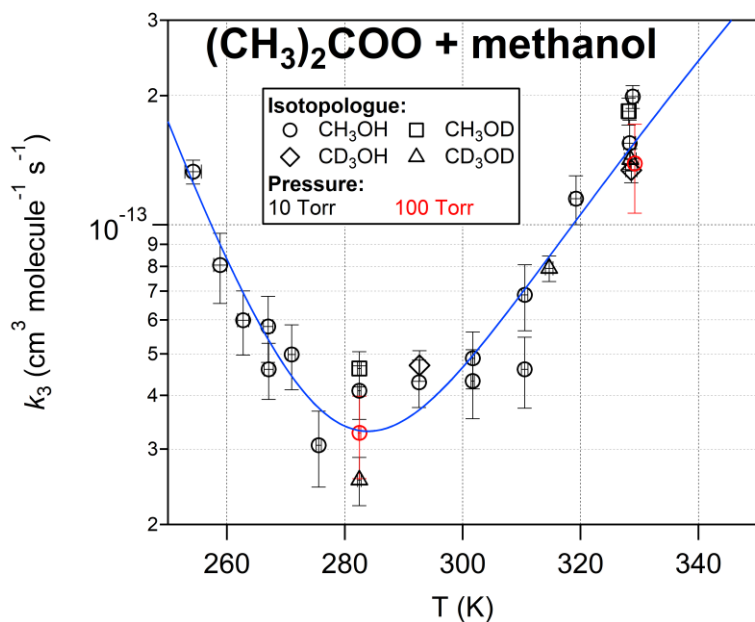
208



209

210 **Fig. 2.** The bimolecular rate coefficients for the reactions of methanol and ethanol with CH_2OO
 211 exhibit a similar negative temperature dependence. Solid lines represent modified Arrhenius fits to
 212 data (see Eqs. III and IV). Error bars represent 2σ statistical uncertainty for rate coefficients and 1σ for
 213 temperature.

214



215

216 **Fig. 3.** The bimolecular rate coefficient for the reaction of methanol with $(\text{CH}_3)_2\text{COO}$ exhibits both
 217 positive and negative temperature dependent regimes. The solid line represents a sum of two AT^n -type
 218 expressions (see Eq. V). Error bars represent 2σ statistical uncertainty for rate coefficients and 1σ for
 219 temperature.

220

221

222 3.1. Reactions of CH₂OO + CH₃OH and C₂H₅OH

223 Reaction 1, CH₂OO + CH₃OH, is the simplest of the reactions studied, with both reactants possessing
224 one carbon atom. This reaction is expected to proceed through an insertion mechanism which
225 produces CH₃OCH₂OOH (MMHP).¹⁹

226 Fig. 2 shows the bimolecular rate coefficient, k_1 , plotted as a function of temperature. These data are
227 tabulated together with the experimental conditions in Table S1. From Fig. 2, it is apparent that there
228 is a negative temperature dependence, no apparent dependence on pressure and that individual
229 determinations of k_1 are highly reproducible. The high precision of the data allows a weak curvature
230 to be observed, which was fitted using a modified Arrhenius expression, yielding the following
231 expression for the temperature dependence of k_1 :

$$232 k_1(T) = 3.7 \pm 1.4 \times 10^{-21} T^2 \exp(1710 \pm 103/T) \text{ (III)}$$

233 The overall negative temperature dependence suggests that Reaction 1 proceeds through a pre-
234 reactive complex in the entrance channel.⁴⁴

235 Reaction 2, CH₂OO + C₂H₅OH, was found to possess a similar rate coefficient to Reaction 1. Fig. 2
236 also shows k_2 vs temperature, with kinetic data and experimental conditions tabulated in Table S2.
237 The precisions of the rate coefficient measurements approach those of Reaction 1, allowing
238 observation of some curvature in the temperature dependence, which was fitted with the following
239 modified Arrhenius expression:

$$240 k_2(T) = 4.2 \pm 2.2 \times 10^{-21} T^2 \exp(1717 \pm 145/T) \text{ (IV)}$$

241 Both the A -factor and the activation energy (E_a/R) are similar to those obtained for Reaction 1,
242 indicating that the carbon chain length on the alcohol does not have a strong influence over the
243 reaction rate. Again, the formation of a pre-reactive complex in the initial reaction step is expected to
244 be responsible for the negative temperature dependence observed.

245 3.2. Reaction of (CH₃)₂COO + CH₃OH

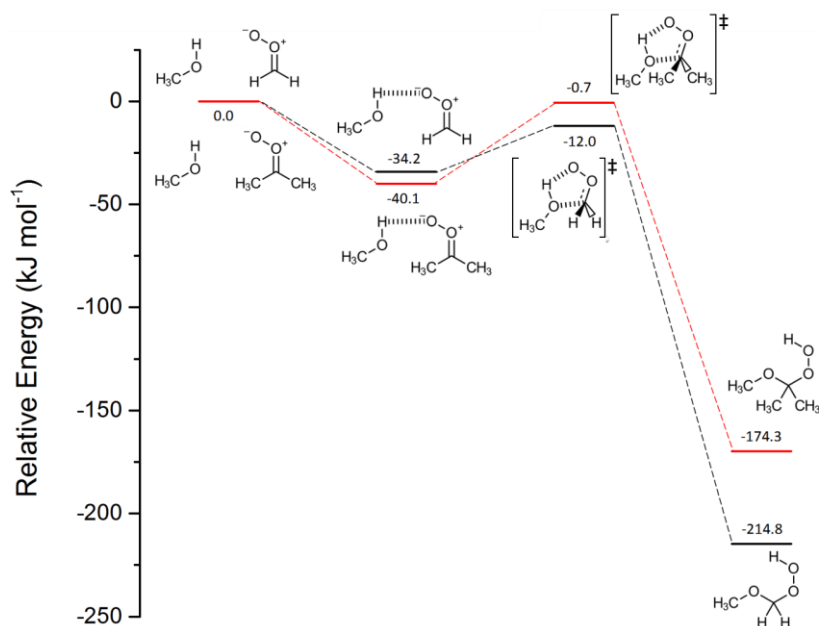
246 Fig. 3 shows a plot of k_3 vs temperature for Reaction (3) (CH₃)₂COO + CH₃OH, with kinetic data and
247 experimental conditions provided in Table S3. In contrast to Reactions 1 and 2, Reaction 3 shows an
248 overall slower reaction rate with a strongly curved temperature dependence. In this instance, the
249 curvature is such that the data are best described with a more complicated function, and a sum of two
250 expressions was used to describe both the positive and negative temperature-dependent components to
251 the overall rate coefficient:

$$252 k_3(T) = 6.07 \times 10^{-33} T^{3.87} \exp(5852/T) + 5.82 \times 10^{-16} T^{2.92} \exp(-3741/T) \text{ (V)}$$

253 Because of the complexity of the above expression, these optimized values should not be considered
254 to form a unique solution, and *A*-factors and activation energies should be treated with caution.
255 However, taken at face value, the temperature dependencies therein are both highly positive and
256 negative respectively. One interpretation of the positive temperature dependent component of this
257 reaction is the agency of a hydrogen abstraction mechanism that operates parallel to the generally
258 accepted insertion mechanism that forms AAAHs in these reactions.^{18-20, 45} To investigate this
259 possibility further, rate coefficients were determined for a suite of deuterated isotopologues of
260 methanol. As can be seen from Fig. 3, no significant differences were observed between the
261 isotopologues. This result indicates that hydrogen abstraction does not make a significant
262 contribution to the overall rate coefficient under these conditions, and implies that the differences are
263 likely to result solely from dissimilarities on the potential energy surfaces for the insertion reactions
264 (see the following section for further discussion). In a pre-reactive complex-forming reaction such as
265 this, there remains the potential for interfering absorption by the complex at the probe wavelength to
266 affect the retrieved decay profiles. A kinetic analysis is presented in the SI, from which we conclude
267 that such an outcome is unlikely.

268 **4. Discussion and supporting calculations**

269 The similarity between $k(T)$ for Reactions 1 and 2 indicates that the size of the alkyl chain of the
270 alcohol has little effect on the rate coefficient for these reactions, and any differences appear to be
271 limited to the *A*-factor. That deuteration of the alcohol moiety has no discernible effect on Reaction 3
272 further implies that H/D transfer does not have a strong impact on the overall rate coefficient. In
273 contrast, the substitution about the CI has a large influence over the reaction rate. One way of
274 rationalizing this observation is that the barrier to forming the transition state that leads to products is
275 higher in the case of Reaction 3. This hypothesis is supported by potential energy calculations for
276 Reactions 1 and 3, shown in Fig. 4, which suggest that both Reactions 1 and 3 form pre-reactive
277 complexes that are stabilized by a single hydrogen bond between the hydrogen of the alcohol moiety
278 and the terminal oxygen of the CI moiety. The barrier to forming AAAH products is found to be
279 submerged in both Reactions 1 and 3, however, in the latter case, the transition state is very close to
280 the energy of reactants. Furthermore, the pre-reactive complex is ~ 6 kJ mol⁻¹ lower in energy than in
281 Reaction 1, demonstrating that the local minimum in which the pre-reactive complex resides is
282 significantly deeper in the case of Reaction 3.



283

284 **Fig. 4.** Potential energy calculations for the reactions of methanol with CH_2OO (black) and
 285 $(\text{CH}_3)_2\text{COO}$ (red). For CH_2OO , a lower barrier is observed, whereas for $(\text{CH}_3)_2\text{COO}$, the barrier that is
 286 encountered by reactants coming out of the pre-reactive complex energy well is significantly higher,
 287 which might explain the complicated temperature dependence observed for this reaction. Optimized
 288 structures for each of these species and complexes can be found in the SI.

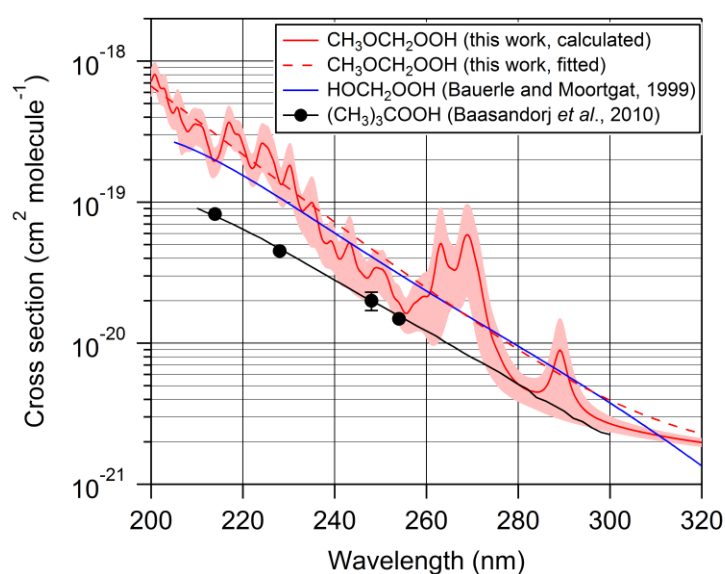
289

290 No absolute kinetic measurements are available in the literature with which Reactions 1–3 can be
 291 compared, although the rate of reaction between methanol and the C_{13} CIs produced from 1-
 292 tetradecene ozonolysis has been determined relative to the reaction with heptanoic acid²⁰. It is
 293 necessary to make several assumptions to put this relative rate onto the absolute scale (see Section 6
 294 for a full treatment), and once performed, yields rate coefficients that are a factor of ~2 larger than the
 295 absolute determinations of this work. Given that at least some of this difference may be physical
 296 between the C_{13} CIs and the smaller CIs of this work, and that no major cancellation of errors results
 297 from these assumptions, the level of agreement is satisfactory. This finding indicates that larger CIs –
 298 more representative of those formed in the atmosphere by ozonolysis and less likely to be consumed
 299 rapidly by water – behave in a similar way to the smaller CIs that are presented here. This comparison
 300 also shows that static chamber-based measurements can provide a suitable alternative to these
 301 absolute measurements, which become rapidly limited by vapour pressure as the size of carbon
 302 backbone of alkyl *gem*-diiodides increases⁴⁶.

303 5. Atmospheric implications.

304 Based on the large flux of methanol to the atmosphere, it is clear that Reactions 1 and 3 cannot
 305 represent an important tropospheric methanol sink. Accordingly, this discussion focusses on the
 306 products of these reactions, the AAAHs. Two main loss processes are considered here, the photolytic
 307 loss and the loss by reaction with OH radicals.

308 The UV absorption spectra of these peroxides have not been studied previously and in order to assess
309 their photolysis lifetimes, a calculated spectrum for MMHP was obtained through the nuclear
310 ensemble method described in the Methods section. Fig. 5 compares this calculated spectrum with
311 experimentally determined spectra for similar hydroperoxides available in the literature⁴⁷⁻⁴⁸. MMHP
312 was found to possess 4 low energy conformers, and the spectrum in Fig. 5 represents an average that
313 is weighted according to the abundance of each of these conformers (for the conformer-specific
314 spectra and their free energies, see SI). A striking similarity was observed between the computed
315 absorption spectrum of MMHP and the most closely analogous compound, hydroxymethyl
316 hydroperoxide, and as with this compound, the photolysis lifetime is therefore expected to be ~4 days
317⁴⁸.

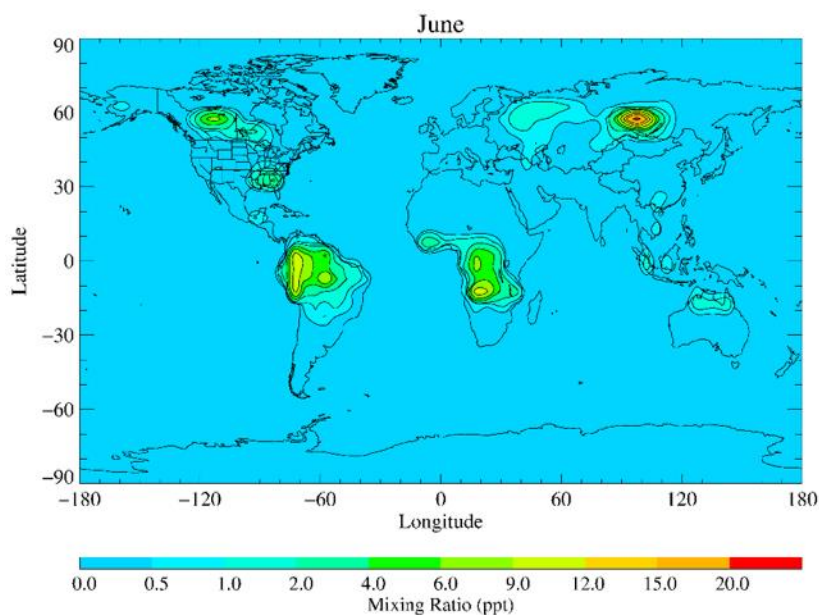


318

319 **Fig. 5.** Calculated UV absorption cross section for the simplest α -alkoxyalkyl hydroperoxide
320 (AAAH), methoxymethyl hydroperoxide (MMHP). A close similarity is observed between MMHP
321 and the literature measurement for hydroxymethyl hydroperoxide, suggesting a commonality in the
322 photochemistry of AAAHs.

323

324 This lifetime is long enough for oxidation by OH to become competitive. Although no rate
325 coefficients of AAAHs + OH are available in the literature, measurements of other hydroperoxides
326 indicate that the peroxidic hydrogen will be the dominant reactive site, with overall rate coefficients
327 that range from $\sim 2\text{--}6 \times 10^{-12} \text{ cm}^3 \text{ molecule}^{-1} \text{ s}^{-1}$ at room temperature^{47, 49-52} and no clear dependence on
328 alkyl substitution. With the additional ether functionality of AAAHs, it is expected that these
329 hydroperoxides will tend towards the more reactive end, and if $6 \times 10^{-12} \text{ cm}^3 \text{ molecule}^{-1} \text{ s}^{-1}$ is
330 representative of the AAAHs, this leads to a lifetime of ~ 2 days assuming an average OH
331 concentration of $1 \times 10^6 \text{ molecule cm}^{-3}$. Reaction with OH will therefore be the main removal process,
332 but photolysis will also be significant.

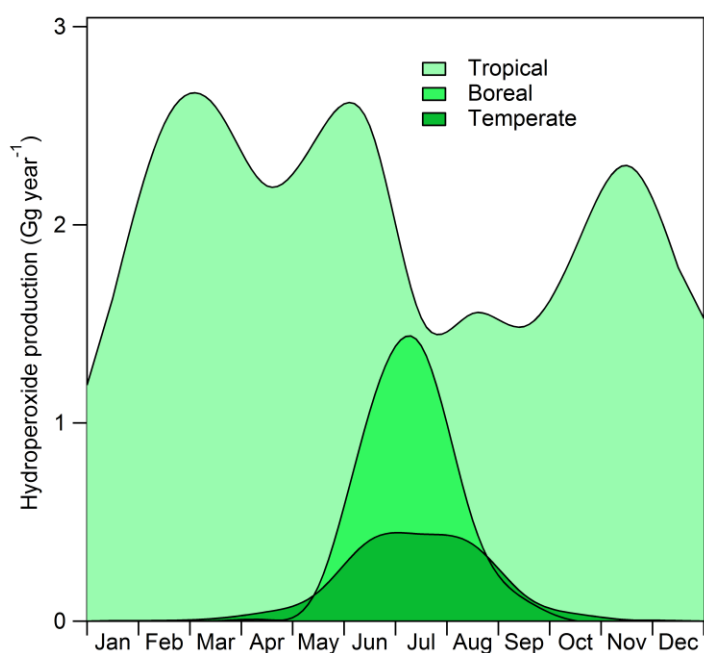


333

334 **Fig. 6.** The global distribution of AAAHs formed in the atmosphere for the month of June. A strong
 335 colocation between AAAHs and the productive forested regions is observed, which is a consequence
 336 of the large terrestrial biospheric source of methanol and alkenes in these areas.

337

338 These atmospheric sinks of AAAHs were incorporated into a global chemistry transport modelling
 339 simulation, together with the source terms described in the Section 2.4 (details on the rate coefficients
 340 employed can be found in Table S4). Global mixing ratios of AAAHs are provided in Fig. 6 for the
 341 month of June, when the biogenic emissions of methanol and CI precursors from the boreal forests are
 342 at a maximum. Fig. 7 shows monthly production rates, indicating that the tropical forests represent a
 343 dominant source throughout the year (24 Gg yr^{-1}), with a minimum between July and September,
 344 during the dry season in the southern tropics. By contrast the boreal forests produce a maximum
 345 between June and August, falling off rapidly on either side, with an annual flux of 3 Gg yr^{-1} .
 346 Temperate forests are the smallest source of AAAHs considered, with a production rate of 2 Gg yr^{-1} ,
 347 showing a similar seasonality to the boreal forests.



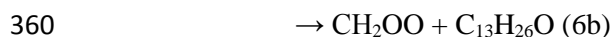
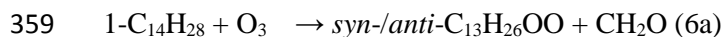
348

349 **Fig. 7.** The production of AAHs over the course of a year. Whereas tropical forests represent a
 350 dominant source throughout the year, boreal and temperate forests only contribute significantly during
 351 the northern hemispheric summer.

352

353 Although the present calculations suggest that AAHs will constitute a radical source in the
 354 troposphere, the formation of larger, more functionalized AAHs derived from the reactions of more
 355 complicated CIs, alcohols, or the secondary oxidation of primary AAHs may have a subtler role to
 356 play in the formation of SOA.

357 **6. Comparison with literature measurements.** Tobias and Ziemann²⁰ reported a room temperature
 358 relative rate for the reaction of a C₁₃ Criegee intermediate produced from 1-tetradecene ozonolysis:

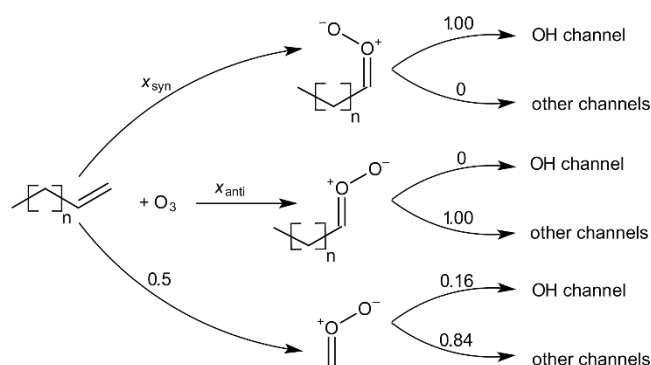


361 where heptanoic acid was employed as a reference reagent. Given that Reaction 6 produces both *syn*
 362 and *anti* conformers, this relative rate is interpreted as follows:

363
$$\frac{(k_{\text{syn-C}_{13}\text{H}_{26}\text{OO} + \text{CH}_3\text{OH}} \cdot x_{\text{syn}}) + (k_{\text{anti-C}_{13}\text{H}_{26}\text{OO} + \text{CH}_3\text{OH}} \cdot (1 - x_{\text{syn}}))}{k_{\text{syn-}/\text{anti-C}_{13}\text{H}_{26}\text{OO} + \text{heptanoic acid}}} = 0.0013$$
 (VI)

364 Comparison of the current results with their measurement, necessitates several assumptions. Firstly,
 365 $k_{\text{syn-}/\text{anti-C}_{13}\text{H}_{26}\text{OO} + \text{heptanoic acid}}$ is taken to be a generic rate coefficient of $1 \times 10^{-10} \text{ cm}^3 \text{ molecule}^{-1} \text{ s}^{-1}$
 366 for all organic acid + CI reactions, with no conformer dependence ascribed⁹. Secondly, in the absence

367 of experimental data, an assumption must be made regarding the molar branching ratio for formation
 368 of the *syn* and *anti* CIs, x_{syn} and $1 - x_{syn}$ in Eq. VI. One way to approach this is to take the OH yield
 369 from analogous terminal alkenes:



370

371 Scheme 1

372 Scheme 1 shows how OH radicals are produced from long-chain terminal alkene ozonolysis. Terminal
 373 alkenes such as 1-hexene, 1-heptene and 1-octene have overall OH yields from ozonolysis of ~ 0.33 .⁵³⁻
 374 ⁵⁴ These compounds are known to produce CH_2OO in a molar yield ($x_{\text{CH}_2\text{OO}}$) of ~ 0.5 .⁵³ The OH yield
 375 of CH_2OO produced through ozonolysis has been determined to be 0.16.⁵³ Rickard et al.⁵⁴ recommend
 376 that *syn*-CIs have a unit OH yield whereas *anti*-CIs do not yield OH, and the overall OH yield can
 377 therefore be described as follows:

$$378 \quad 1.0 \cdot x_{syn} + (0.16 \cdot x_{\text{CH}_2\text{OO}}) = 0.33 \quad (\text{VII})$$

379 which gives a value for x_{syn} of 0.25. Since the three possible CIs formed must sum to a yield of one,
 380 the yield of *anti*-CI (x_{anti}) will be 0.25 also.

381 The third assumption is that the ratio of rate coefficients for *syn*- and *anti*- $\text{C}_{13}\text{H}_{26}\text{OO}$ is similar to that
 382 for the k (CH_3)₂COO and $\text{CH}_2\text{OO} + \text{CH}_3\text{OH}$ measured in this study (0.42 at 298 K); in the case of
 383 (CH_3)₂COO, the terminal oxygen atom always faces towards an alkyl substitution and is considered to
 384 be representative of a purely *syn*-CI, whereas CH_2OO never faces an alkyl substitution and is
 385 considered to be purely *anti* in character. Since the relative rate coefficient of Tobias and Ziemann²⁰
 386 only considers the fate of the $\text{C}_{13}\text{H}_{26}\text{OO}$ CIs, the above values of 0.25 are effectively doubled, and by
 387 accounting for the ratio of k_1 and k_3 from this study, Eq. VI is simplified as follows:

$$388 \quad \frac{k_{anti}^{0.71}}{1 \times 10^{-10}} = 0.0013 \quad (\text{VIII})$$

389 from which individual rate coefficient values of 2×10^{-13} and $8 \times 10^{-14} \text{ cm}^3 \text{ molecule}^{-1} \text{ s}^{-1}$ can be
 390 obtained for *anti*- and *syn*- $\text{C}_{13}\text{H}_{26}\text{OO}$ respectively. These values are a factor of 2 larger than the rate
 391 coefficients determined in this work. Given that at least some of these differences may be physical
 392 between the C_{13} CIs and the smaller CIs that have been studied here, and assuming that no major

393 cancellation of errors results from the above assumptions, the level of agreement is satisfactory. This
394 comparison suggests that the static chamber ozonolysis experiments, if conducted under the right
395 conditions, are a reliable source of kinetic data for the reactions of large CIs that cannot be accessed
396 through the direct methodology employed in this work.

397 7. Conclusions

398 Direct experimental rate coefficient measurements for the reactions of CH_2OO and $(\text{CH}_3)_2\text{COO} +$
399 methanol and that of $\text{CH}_2\text{OO} +$ ethanol are presented. Experimental conditions were varied between
400 temperatures of 254 and 329 K, and pressures of 10 and 100 Torr (N_2), with no evidence of pressure
401 dependence and a strong non-Arrhenius temperature dependence observed in all cases. The rate
402 coefficient of $(\text{CH}_3)_2\text{COO} +$ methanol exhibited both a negative and positive temperature-dependent
403 component, which may in part be explained by a higher barrier encountered by the pre-reactive
404 complex as it proceeds to product formation. It is acknowledged, however, that this alone is
405 insufficient to explain the extent of the temperature dependence observed, and a more rigorous
406 theoretical treatment is required. The insertion reactions by which CIs react with alcohols produce α -
407 alkoxyalkyl hydroperoxides (AAAHs). The calculated UV cross section of a representative of these
408 species, methoxymethyl hydroperoxide (MMHP), is found to be similar to other peroxides, indicating
409 that whilst tropospheric photolysis is an important sink for these species, oxidation and deposition are
410 likely to be competitive. Based on these findings, a global chemistry transport model is used to
411 estimate the abundance and flux of AAAHs into the global atmosphere. A total flux of $\sim 30 \text{ Gg Yr}^{-1}$ is
412 obtained, with most production occurring in the tropical forests, where biogenic methanol and alkene
413 emissions are both high.

414 Supporting Information

415 Tabulated experimental data and conditions. Computational details for UV cross section and potential
416 energy calculations. Kinetic parameters employed in atmospheric chemical modelling. NMR spectra
417 for $(\text{CH}_3)_2\text{CI}_2$ sample. Kinetic analysis of experimental observations.

418 **Acknowledgements.** Funding for this work by NERC grants NE/K004905/1 and NE/P013104/1 is
419 gratefully acknowledged. MRM, JMB and BFEC are supported by Marie Skłodowska-Curie
420 Individual Fellowships HOMER (702794), NPTC (701593) and NAMDIA (710355) respectively. We
421 thank Prof. G.C. Lloyd-Jones and Drs C. Nottingham and T. West (University of Edinburgh) for the
422 2,2-diiodopropane sample.

423 References

424 1. Johnson, D.; Marston, G., The Gas-phase Ozonolysis of Unsaturated Volatile Organic
425 Compounds in the Troposphere. *Chem. Soc. Rev.* **2008**, 37 (4), 699-716.

- 426 2. Anglada, J. M.; Gonzalez, J.; Torrent-Sucarrat, M., Effects of the Substituents on the
427 Reactivity of Carbonyl Oxides. A Theoretical Study on the Reaction of Substituted Carbonyl Oxides
428 with Water. *Phys. Chem. Chem. Phys.* **2011**, *13* (28), 13034-13045.
- 429 3. Smith, M. C.; Chang, C. H.; Chao, W.; Lin, L. C.; Takahashi, K.; Boering, K. A.; Lin, J. J.
430 M., Strong Negative Temperature Dependence of the Simplest Criegee Intermediate CH₂OO Reaction
431 with Water Dimer. *J. Phys. Chem. Lett.* **2015**, *6* (14), 2708-2713.
- 432 4. Huang, H. L.; Chao, W.; Lin, J. J. M., Kinetics of a Criegee Intermediate that would Survive
433 High Humidity and may Oxidize Atmospheric SO₂. *P. Natl. Acad. Sci. USA* **2015**, *112* (35), 10857-
434 10862.
- 435 5. Chhantyal-Pun, R.; Davey, A.; Shallcross, D. E.; Percival, C. J.; Orr-Ewing, A. J., A Kinetic
436 Study of the CH₂OO Criegee Intermediate Self-reaction, Reaction with SO₂ and Unimolecular
437 Reaction using Cavity Ring-down Spectroscopy. *Phys. Chem. Chem. Phys.* **2015**, *17* (5), 3617-3626.
- 438 6. Novelli, A.; Hens, K.; Ernest, C. T.; Martinez, M.; Nölscher, A. C.; Sinha, V.; Paasonen, P.;
439 Petäjä, T.; Sipilä, M.; Elste, T.; Plass-Dülmer, C.; Phillips, G. J.; Kubistin, D.; Williams, J.;
440 Vereecken, L.; Lelieveld, J.; Harder, H., Estimating the atmospheric concentration of Criegee
441 intermediates and their possible interference in a FAGE-LIF instrument. *Atmos. Chem. Phys.* **2017**,
442 *17*, 7807-7826.
- 443 7. Berndt, T.; Jokinen, T.; Sipilä, M.; Mauldin, R. L.; Herrmann, H.; Stratmann, F.; Junninen,
444 H.; Kulmala, M., H₂SO₄ Formation from the Gas-phase Reaction of Stabilized Criegee Intermediates
445 with SO₂: Influence of Water Vapour Content and Temperature. *Atmos. Environ.* **2014**, *89*, 603-612.
- 446 8. Mauldin, R. L.; Berndt, T.; Sipilä, M.; Paasonen, P.; Petaja, T.; Kim, S.; Kurten, T.;
447 Stratmann, F.; Kerminen, V. M.; Kulmala, M., A new atmospherically relevant oxidant of sulphur
448 dioxide. *Nature* **2012**, *488* (7410), 193-196.
- 449 9. Welz, O.; Eskola, A. J.; Sheps, L.; Rotavera, B.; Savee, J. D.; Scheer, A. M.; Osborn, D. L.;
450 Lowe, D.; Booth, A. M.; Xiao, P.; Khan, M. A. H.; Percival, C. J.; Shallcross, D. E.; Taatjes, C. A.,
451 Rate Coefficients of C1 and C2 Criegee Intermediate Reactions with Formic and Acetic Acid Near the
452 Collision Limit: Direct Kinetics Measurements and Atmospheric Implications. *Angew. Chem. Int. Ed.*
453 **2014**, *53* (18), 4547-4550.
- 454 10. Chhantyal-Pun, R.; McGillen, M. R.; Beames, J. M.; Khan, M. A. H.; Percival, C. J.;
455 Shallcross, D. E.; Orr-Ewing, A. J., Temperature Dependence of the Rates of Reaction of
456 Trifluoroacetic Acid with Criegee Intermediates. *Angew. Chem. Int. Ed.* **2017**, *56* (31), 9044-9047.
- 457 11. Buras, Z. J.; Elsamra, R. M. I.; Jalan, A.; Middaugh, J. E.; Green, W. H., Direct Kinetic
458 Measurements of Reactions between the Simplest Criegee Intermediate CH₂OO and Alkenes. *J. Phys.*
459 *Chem. A* **2014**, *118* (11), 1997-2006.
- 460 12. Elsamra, R. M. I.; Jalan, A.; Buras, Z. J.; Middaugh, J. E.; Green, W. H., Temperature- and
461 Pressure-dependent Kinetics of CH₂OO + CH₃COCH₃ and CH₂OO + CH₃CHO: Direct Measurements
462 and Theoretical Analysis. *Int. J. Chem. Kinet.* **2016**, *48* (8), 474-488.
- 463 13. Sakamoto, Y.; Yajima, R.; Inomata, S.; Hirokawa, J., Water Vapour Effects on Secondary
464 Organic Aerosol Formation in Isoprene Ozonolysis. *Phys. Chem. Chem. Phys.* **2017**, *19* (4), 3165-
465 3175.
- 466 14. Vereecken, L.; Rickard, A. R.; Newland, M. J.; Bloss, W. J., Theoretical Study of the
467 Reactions of Criegee Intermediates with Ozone, Alkylhydroperoxides, and Carbon Monoxide. *Phys.*
468 *Chem. Chem. Phys.* **2015**, *17* (37), 23847-23858.
- 469 15. Goldan, P. D.; Kuster, W. C.; Fehsenfeld, F. C.; Montzka, S. A., The Observation of a C5
470 Alcohol Emission in a North-American Pine Forest. *Geophys. Res. Lett.* **1993**, *20* (11), 1039-1042.
- 471 16. Stavrou, T.; Guenther, A.; Razavi, A.; Clarisse, L.; Clerbaux, C.; Coheur, P. F.; Hurtmans,
472 D.; Karagulian, F.; De Maziere, M.; Vigouroux, C.; Amelynck, C.; Schoon, N.; Laffineur, Q.;
473 Heinesch, B.; Aubinet, M.; Rinsland, C.; Muller, J. F., First Space-based Derivation of the Global
474 Atmospheric Methanol Emission Fluxes. *Atmos. Chem. Phys.* **2011**, *11* (10), 4873-4898.
- 475 17. Leather, K. E.; McGillen, M. R.; Cooke, M. C.; Utembe, S. R.; Archibald, A. T.; Jenkin, M.
476 E.; Derwent, R. G.; Shallcross, D. E.; Percival, C. J., Acid-yield Measurements of the Gas-phase
477 Ozonolysis of Ethene as a Function of Humidity using Chemical Ionisation Mass Spectrometry
478 (CIMS). *Atmos. Chem. Phys.* **2012**, *12* (1), 469-479.
- 479 18. Dussault, P.; Sahli, A., 2-Methoxyprop-2-yl Hydroperoxide - a Convenient Reagent for the
480 Synthesis of Hydroperoxides and Peracids. *J. Org. Chem.* **1992**, *57* (3), 1009-1012.

- 481 19. Neeb, P.; Horie, O.; Moortgat, G. K., Gas-phase Ozonolysis of Ethene in the Presence of
482 Hydroxylic Compounds. *Int. J. Chem. Kinet.* **1996**, 28 (10), 721-730.
- 483 20. Tobias, H. J.; Ziemann, P. J., Kinetics of the Gas-phase Reactions of Alcohols, Aldehydes,
484 Carboxylic Acids, and Water with the C13 Stabilized Criegee Intermediate Formed from Ozonolysis
485 of 1-Tetradecene. *J. Phys. Chem. A* **2001**, 105 (25), 6129-6135.
- 486 21. Welz, O.; Savee, J. D.; Osborn, D. L.; Vasu, S. S.; Percival, C. J.; Shallcross, D. E.; Taatjes,
487 C. A., Direct Kinetic Measurements of Criegee Intermediate (CH₂OO) Formed by Reaction of CH₂I
488 with O₂. *Science* **2012**, 335 (6065), 204-207.
- 489 22. Frisch, M. J.; Trucks, G. W.; Schlegel, H. B.; Scuseria, G. E.; Robb, M. A.; Cheeseman, J. R.;
490 Scalmani, G.; Barone, V.; Petersson, G. A.; Nakatsuji, H.; Li, X.; Caricato, M.; Marenich, A.; Bloino,
491 J.; Janesko, B. G.; Gomperts, R.; Mennucci, B.; Hratchian, H. P.; Ortiz, J. V.; Izmaylov, A. F.;
492 Sonnenberg, J. L.; Williams-Young, D.; Ding, F.; Lipparini, F.; Egidi, F.; Goings, J.; Peng, B.;
493 Petrone, A.; Henderson, T.; Ranasinghe, D.; Zakrzewski, V. G.; Gao, J.; Rega, N.; Zheng, G.; Liang,
494 W.; Hada, M.; Ehara, M.; Toyota, K.; Fukuda, R.; Hasegawa, J.; Ishida, M.; Nakajima, T.; Honda, Y.;
495 Kitao, O.; Nakai, H.; Vreven, T.; Throssell, K.; Montgomery, J. A.; Peralta, J. J. E.; Ogliaro, F.;
496 Bearpark, M.; Heyd, J. J.; Brothers, E.; Kudin, K. N.; Staroverov, V. N.; Keith, T.; Kobayashi, R.;
497 Normand, J.; Raghavachari, K.; Rendell, A.; Burant, J. C.; Iyengar, S. S.; Tomasi, J.; Cossi, M.;
498 Millam, J. M.; Klene, M.; Adamo, C.; Cammi, R.; Ochterski, J. W.; Martin, R. L.; Morokuma, K.;
499 Farkas, O.; Foresman, J. B.; Fox, D. J., *Gaussian 09, Revision D.01*. Gaussian, Inc.: Wallingford, CT.,
500 2016.
- 501 23. Werner, H. J.; Knowles, P. J.; Knizia, G.; Manby, F. R.; Schütz, M.; Celani, P.; Györfy, W.;
502 Kats, D.; Korona, T.; Lindh, R.; Mitrushenkov, A.; Rauhut, G.; Shamasundar, K. R.; Adler, T. B.;
503 Amos, R. D.; Bernhardsson, A.; Berning, A.; Cooper, D. L.; Deegan, M. J. O.; Dobbyn, A. J.; Eckert,
504 F.; Goll, E.; Hampel, C.; Hesselmann, A.; Hetzer, G.; Hrenar, T.; Jansen, G.; Köppl, C.; Liu, Y.;
505 Lloyd, A. W.; Mata, R. A.; May, A. J.; McNicholas, S. J.; Meyer, W.; Mura, M. E.; Nicklaß, A.;
506 O'Neill, D. P.; Palmieri, P.; Peng, D.; Pflüger, K.; Pitzer, R.; Reiher, M.; Shiozaki, T.; Stoll, H.;
507 Stone, A. J.; Tarroni, R.; Thorsteinsson, T.; Wang, M., *MOLPRO is a package of ab initio programs*
508 *written by*.
- 509 24. Miliordos, E.; Xantheas, S. S., The Origin of the Reactivity of the Criegee Intermediate:
510 Implications for Atmospheric Particle Growth. *Angew. Chem. Int. Ed.* **2016**, 55 (3), 1015-1019.
- 511 25. Frisch, M. J.; Head-Gordon, M.; Pople, J. A., A Direct MP2 Gradient-Method. *Chem. Phys.*
512 *Lett.* **1990**, 166 (3), 275-280.
- 513 26. Head-Gordon, M.; Head-Gordon, T., Analytic MP2 Frequencies without 5th-Order Storage -
514 Theory and Application to Bifurcated Hydrogen-Bonds in the Water Hexamer. *Chem. Phys. Lett.*
515 **1994**, 220 (1-2), 122-128.
- 516 27. Head-Gordon, M.; Pople, J. A.; Frisch, M. J., MP2 Energy Evaluation by Direct Methods.
517 *Chem. Phys. Lett.* **1988**, 153 (6), 503-506.
- 518 28. Møller, C.; Plesset, M. S., Note on an Approximation Treatment for Many-electron Systems.
519 *Phys. Rev.* **1934**, 46 (7), 0618-0622.
- 520 29. Dunning, T. H., Gaussian-Basis Sets for Use in Correlated Molecular Calculations .1. The
521 Atoms Boron through Neon and Hydrogen. *J. Chem. Phys.* **1989**, 90 (2), 1007-1023.
- 522 30. Barbatti, M.; Aquino, A. J. A.; Lischka, H., The UV Absorption of Nucleobases: Semi-
523 classical Ab Initio Spectra Simulations. *Phys. Chem. Chem. Phys.* **2010**, 12 (19), 4959-4967.
- 524 31. Barbatti, M.; Sen, K., Effects of Different Initial Condition Samplings on Photodynamics and
525 Spectrum of Pyrrole. *Int. J. Quantum Chem.* **2016**, 116 (10), 762-771.
- 526 32. Crespo-Otero, R.; Barbatti, M., Spectrum Simulation and Decomposition with Nuclear
527 Ensemble: Formal Derivation and Application to Benzene, Furan and 2-Phenylfuran. *Theor. Chem.*
528 *Acc.* **2012**, 131 (6).
- 529 33. Barbatti, M.; Granucci, G.; Ruckebauer, M.; Plasser, F.; Crespo-Otero, R.; Pittner, J.;
530 Persico, M.; Lischka, H. NEWTON-X: A Package for Newtonian Dynamics Close to the Crossing
531 Seam, Version 1.4. www.newtonx.org.
- 532 34. Barbatti, M.; Ruckebauer, M.; Plasser, F.; Pittner, J.; Granucci, G.; Persico, M.; Lischka, H.,
533 Newton-X: A Surface-hopping Program for Nonadiabatic Molecular Dynamics. *Wires Comput Mol*
534 *Sci* **2014**, 4 (1), 26-33.

535 35. Christiansen, O.; Koch, H.; Jorgensen, P., The 2nd-Order Approximate Coupled-Cluster
536 Singles and Doubles Model CC2. *Chem. Phys. Lett.* **1995**, *243* (5-6), 409-418.

537 36. Grimme, S., Improved Second-order Møller-Plesset Perturbation Theory by Separate Scaling
538 of Parallel- and Antiparallel-spin Pair Correlation Energies. *J. Chem. Phys.* **2003**, *118* (20), 9095-
539 9102.

540 37. Hellweg, A.; Grün, S. A.; Hättig, C., Benchmarking the Performance of Spin-component
541 Scaled CC2 in Ground and Electronically Excited States. *Phys. Chem. Chem. Phys.* **2008**, *10* (28),
542 4119-4127.

543 38. Furche, F.; Ahlrichs, R.; Hättig, C.; Klopper, W.; Sierka, M.; Weigend, F., Turbomole. *Wires*
544 *Comput Mol Sci* **2014**, *4* (2), 91-100.

545 39. Korona, T.; Werner, H. J., Local Treatment of Electron Excitations in the EOM-CCSD
546 Method. *J. Chem. Phys.* **2003**, *118* (7), 3006-3019.

547 40. Utembe, S. R.; Cooke, M. C.; Archibald, A. T.; Jenkin, M. E.; Derwent, R. G.; Shallcross, D.
548 E., Using a Reduced Common Representative Intermediates (CRIv2-R5) Mechanism to Simulate
549 Tropospheric Ozone in a 3-D Lagrangian Chemistry Transport Model. *Atmos. Environ.* **2010**, *44* (13),
550 1609-1622.

551 41. Guenther, A. B.; Jiang, X.; Heald, C. L.; Sakulyanontvittaya, T.; Duhl, T.; Emmons, L. K.;
552 Wang, X., The Model of Emissions of Gases and Aerosols from Nature version 2.1 (MEGAN2.1): An
553 Extended and Updated Framework for Modeling Biogenic Emissions. *Geosci. Model Dev.* **2012**, *5*
554 (6), 1471-1492.

555 42. Percival, C. J.; Welz, O.; Eskola, A. J.; Savee, J. D.; Osborn, D. L.; Topping, D. O.; Lowe,
556 D.; Utembe, S. R.; Bacak, A.; McFiggans, G.; Cooke, M. C.; Xiao, P.; Archibald, A. T.; Jenkin, M.
557 E.; Derwent, R. G.; Riipinen, I.; Mok, D. W. K.; Lee, E. P. F.; Dyke, J. M.; Taatjes, C. A.; Shallcross,
558 D. E., Regional and Global Impacts of Criegee Intermediates on Atmospheric Sulphuric Acid
559 Concentrations and First Steps of Aerosol Formation. *Faraday Discuss.* **2013**, *165*, 45-73.

560 43. Chhantyal-Pun, R.; Welz, O.; Savee, J. D.; Eskola, A. J.; Lee, E. P. F.; Blacker, L.; Hill, H.
561 R.; Ashcroft, M.; Khan, M. A. H.; Lloyd-Jones, G. C.; Evans, L.; Rotavera, B.; Huang, H. F.; Osborn,
562 D. L.; Mok, D. K. W.; Dyke, J. M.; Shallcross, D. E.; Percival, C. J.; Orr-Ewing, A. J.; Taatjes, C. A.,
563 Direct Measurements of Unimolecular and Bimolecular Reaction Kinetics of the Criegee Intermediate
564 (CH₃)₂COO. *J. Phys. Chem. A* **2017**, *121* (1), 4-15.

565 44. Donahue, N. M., Reaction Barriers: Origin and Evolution. *Chem. Rev.* **2003**, *103* (12), 4593-
566 4604.

567 45. Criegee, R., Mechanism of Ozonolysis. *Angew. Chem. Int. Ed.* **1975**, *14* (11), 745-752.

568 46. Yaws, C. L., *The Yaws Handbook of Vapor Pressure: Antoine Coefficients*. 2 ed.; Elsevier:
569 Oxford, 2015.

570 47. Baasandorj, M.; Papanastasiou, D. K.; Talukdar, R. K.; Hasson, A. S.; Burkholder, J. B.,
571 (CH₃)₃COOH (Tert-butyl Hydroperoxide): OH Reaction Rate Coefficients Between 206 and 375 K
572 and the OH Photolysis Quantum Yield at 248 nm. *Phys. Chem. Chem. Phys.* **2010**, *12* (38), 12101-
573 12111.

574 48. Bauerle, S.; Moortgat, G. K., Absorption Cross-sections of HOCH₂OOH Vapor Between 205
575 and 360 nm at 298 K. *Chem. Phys. Lett.* **1999**, *309* (1-2), 43-48.

576 49. Anastasi, C.; Smith, I. W. M., Flash-photolysis Study of Spectra of CH₃O₂ and C(CH₃)₃O₂
577 Radicals and Kinetics of their Mutual Reactions and with NO. *J. Chem. Soc-Faraday Trans. I* **1978**,
578 *74*, 1693-1701.

579 50. Atkinson, R.; Baulch, D. L.; Cox, R. A.; Crowley, J. N.; Hampson, R. F.; Hynes, R. G.;
580 Jenkin, M. E.; Rossi, M. J.; Troe, J. IUPAC Task Group on Atmospheric Chemical Kinetic Data
581 Evaluation. <http://iupac.pole-ether.fr>.

582 51. Blitz, M. A.; Heard, D. E.; Pilling, M. J., Wavelength Dependent Photodissociation of
583 CH₃OOH - Quantum Fields for CH₃O and OH, and Measurement of the OH+CH₃OOH Rate
584 Coefficient. *J. Photochem. Photobiol. A-Chem.* **2005**, *176* (1-3), 107-113.

585 52. Vaghjiani, G. L.; Ravishankara, A. R., Kinetics and Mechanism of OH Reaction with
586 CH₃OOH. *J. Phys. Chem.* **1989**, *93* (5), 1948-1959.

587 53. Atkinson, R., Gas-phase Tropospheric Chemistry of Volatile Organic Compounds 1. Alkanes
588 and Alkenes. *J. Phys. Chem. Ref. Data* **1997**, *26* (2), 215-290.

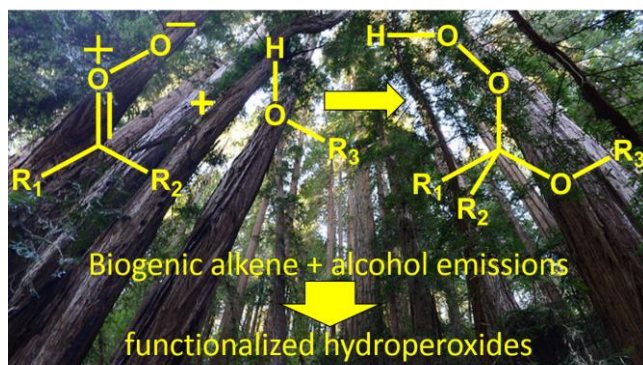
589 54. Rickard, A. R.; Johnson, D.; McGill, C. D.; Marston, G., OH Yields in the Gas-phase
590 Reactions of Ozone with Alkenes. *J. Phys. Chem. A* **1999**, *103* (38), 7656-7664.

591

592

593

594 For TOC only:



595